

Achieving Real-Time LiDAR 3D Object Detection on a Mobile Device

¹Pu Zhao, ²Wei Niu, ¹Geng Yuan, ¹Yuxuan Cai, ³Hsin-Hsuan Sung,
⁴Sijia Liu, ³Xipeng Shen, ²Bin Ren, ¹Yanzhi Wang, ¹Xue Lin

¹Northeastern University, Boston, MA

²William & Mary, Williamsburg, VA

³North Carolina State University, Raleigh, NC

⁴Michigan State University, East Lansing, MI

Abstract—3D object detection is an important task, especially in the autonomous driving application domain. However, it is challenging to support the real-time performance with the limited computation and memory resources on edge-computing devices in self-driving cars. To achieve this, we propose a compiler-aware unified framework incorporating network enhancement and pruning search with the reinforcement learning techniques, to enable real-time inference of 3D object detection on the resource-limited edge-computing devices. Specifically, a generator Recurrent Neural Network (RNN) is employed to provide the unified scheme for both network enhancement and pruning search automatically, without human expertise and assistance. And the evaluated performance of the unified schemes can be fed back to train the generator RNN. The experimental results demonstrate that the proposed framework firstly achieves real-time 3D object detection on mobile devices (Samsung Galaxy S20 phone) with competitive detection performance.

I. INTRODUCTION

There are growing interests in two aspects of the machine learning field. First, various Deep Neural Network (DNN) architectures have served as the fundamental building blocks of machine learning applications due to the superior accuracy performance [17]. Second, the edge-computing devices such as embedded systems, FPGAs, ASIC chips have been serving as the primary carriers of machine learning applications including autonomous driving, wearable health devices, video streaming, etc. [45], [29]. It is desirable and challenging to deploy DNN models on edge devices, targeting for real-time inference performance. Take the 3D object detection on self-driving cars as an example. To ensure driving safety, the 3D detection with point clouds [10] should satisfy the real-time inference requirement when executed on resource-limited GPU devices equipped on self-driving cars, since the more powerful high-end GPUs are too costly and power-hungry to use on vehicles. However, many state-of-the-art DNN models such as VGG-16 [54] and Yolo [4] are computation and memory-intensive for the light-weighted edge computing devices to obtain real-time performance.

To reduce the computation and memory requirements and therefore accelerate the DNN inference execution, DNN model pruning techniques have been used to remove the redundancy in DNN models [57], [19], [22], [23]. Various DNN pruning frameworks explore i) different pruning methods (how to prune) such as magnitude pruning [14] and ADMM pruning

[63], ii) pruning types (what to prune) such as pattern pruning [39] and filter pruning [23], and iii) pruning ratio (how much to prune) [19].

A noteworthy direction is the pattern pruning [39], which prunes kernels according to a predefined pattern set to facilitate compiler optimizations towards higher parallelism for inference execution and therefore superior acceleration. There have been other DNN inference acceleration frameworks on edge devices with compiler optimizations such as Tensorflow-Lite [1], TVM [7], MNN [2], and PyTorch [44], although they focus on unpruned models. Moreover, Winograd [3], [31] could improve the inference speed by transforming tiles of the input and kernel into a modulo polynomials Winograd domain, although the transformations cause certain overhead which may degrade the improvement. This paper makes an observation from all these above-mentioned frameworks that kernel size plays an important role and should be identified as a new network optimization dimension, and therefore proposes to perform the kernel size fine-tuning and adopt Winograd as the key network enhancement techniques to facilitate compiler optimization for inference acceleration.

There are several problems with the existing efforts. First, previous pruning frameworks usually fix the pruning method and pruning type for all the layers in the model without customizing the best-suited pruning type for each layer. Second, there lacks a method to evaluate the inference speed performance of different network enhancements in presence of compiler optimizations. Third, the process of model pruning, network enhancements, and compiler optimization co-design relies heavily on professional expertise and experience, and involves large manual hyperparameter fine-tuning efforts.

On the other hand, Automated Machine Learning (AutoML) [21], [50] has gained ever-increasing interests and attention that tries to automatically solve problems without human assistance under the given computational budget. In AutoML, Neural Architecture Search (NAS) [67], [35], [25], [48] receives notable attention that designs novel network architectures without human expertise that can rival the best human-invented architectures in terms of testing accuracy. NAS makes the architecture design less dependent on human experts with a solid understanding of deep learning as well as the application domain.

To satisfy the real-time inference requirement for 3D object detection with point clouds on edge devices, and inspired by NAS, we propose a compiler-aware unified framework incorporating network enhancement and pruning search with reinforcement learning (RL). The framework automatically generates various unified schemes with a list of network enhancement and pruning actions. Then the performance of the models derived under the unified schemes can be fed back to the generator to maximize the expected rewards. Although there are some other DNN inference acceleration frameworks with compiler optimizations such as Tensorflow-Lite [1], TVM [7] and MNN [2], we are the first to provide support for real-time 3D object detection on mobile GPUs (we use Samsung Galaxy S20 phone here). The contributions are summarized as follows.

- **Unified framework.** We propose a unified framework incorporating network enhancement and pruning search with reinforcement learning for 3D object detection. For the first time, we provide support for real-time 3D object detection on mobile GPUs with compiler optimization.
- **Flexible configuration.** Distinctive from existing works using fixed pruning or network enhancement strategy, our framework enjoys the great flexibility that can be customized and optimized down to the layer level while covering state-of-the-art practices.
- **Compiler awareness.** The framework is able to take into account the effects of compiler optimizations during the search space exploration, through the automatic code generation of compiler with the supports of various pruning and network enhancement techniques.
- **Real-time performance.** To satisfy the inference speed requirement, we take the real-time performance constraint into considerations during the search space exploration as a reward for different schemes. Our experimental results demonstrate that the proposed framework can achieve real-time 3D object detection on mobile devices (Samsung Galaxy S20 phone).

II. RELATED WORK

A. Network Enhancement

Compiler optimization is able to improve the inference speed by utilizing hardware parallelism more efficiently. Thus a new optimization dimension, i.e., kernel size, is introduced as different kernel size of convolutional (CONV) layers lead to different inference speedups under compiler optimization. Besides, changing the kernel size can boost model performance in some cases such as wide activation [61], [62], which first expands features before ReLU functions and then uses linear low-rank convolution that factorizes a large convolution kernel into two low-rank convolution kernels without additional parameters or computation. Thus it is desirable to find the suitable kernel size.

By transforming tiles of the input and kernel into a modulo polynomials Winograd domain, Winograd [31], [3] can reduce the arithmetic complexity of a CONV layer by up to a factor of

4 compared with direct convolution. With Winograd, almost all of the arithmetic is performed by dense matrix multiplications with sufficient dimensions, in order to improve computation efficiency, even with small batch size.

B. DNN Model Pruning

DNNs achieve superior performance on various practical applications such as classification or detection with large storage/computation costs. To simultaneously reduce the storage/computation and accelerate inference speed, DNN model pruning has been proposed during DNN training for reducing the redundancy in DNN weights [57], [19], [22], [23].

a) Pruning Method.: There are various pruning methods including heuristic pruning method [20], [19], [14] such as magnitude pruning [20], [19], [37], and optimization-based pruning method [66], [65], [40] such as Alternating Direction Methods of Multipliers (ADMM) pruning [63], [32]. The heuristic pruning is usually performed in an iterative manner to prune weights with small magnitudes. The optimization-based pruning method normally incorporates a regularization term in loss function to solve pruning problems. Specifically, ADMM pruning [63], [32] incorporates a dynamic regularization penalty to adjust the relative significance of the penalty and the loss, leading to more efficient training.

b) Pruning Type.: There exist a number of different pruning types for each layer, including unstructured pruning [20], [19], [37], and structured pruning [41], [66], [65], [40], [36]. Unstructured pruning removes weights at arbitrary position to significantly decrease the number of weights in DNN model. But the irregularly pruned weight matrix with indices requires additional storage and has limited hardware parallelism. Different from unstructured pruning, many works investigate the structured pruning methods [41], [65], [36] such as filter pruning [23]. The highly regular model structures after pruning are compatible with hardware parallel implementations. But the compression ratio may be limited as pruning the whole filter can cause non-neglectable accuracy degradation. To overcome their weakness, pattern pruning [39], [43] combines kernel pattern pruning with connectivity pruning. It first reserves 4 non-zero weights out of the original 3×3 kernels and then removes the whole redundant kernels and the corresponding connection between the input and output channels. Pattern pruning achieves the benefits of both unstructured and structured pruning while avoiding their weaknesses.

C. Neural Architecture Search

NAS [67] is a popular research direction aiming to automate the design process of DNN architectures for a given task/dataset. NAS strategies have found various neural architectures with state-of-the-art performance outperforming human experts' design on a variety of tasks [5], [35], [34], [38]. Similar to hyperparameter optimization, NAS can often be formulated as a black-box optimization problem [12] and the evaluation of the objective can be very expensive due to the training of the architecture. NAS can adopt various

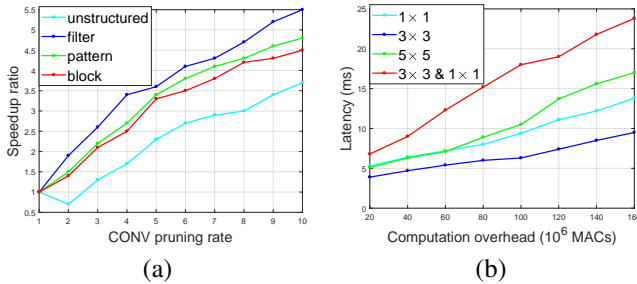


Fig. 1: (a) Speedup ratio v.s. CONV pruning rate for various pruning methods. (b) Latency v.s. computation overhead for various kernel sizes.

methods including RL [67], [34], evolution [56], [13] and gradients [35], [6] to design the search strategies. RL-based NAS [67] trains a RNN with the reinforce loss to generate different the architectures. Evolution-based NAS [56] adopts genetic algorithms such as population generation and offspring elimination to explore different models. Gradient-based NAS [35], [6] proposes a differentiable algorithm and solve the problem with a bilevel optimization.

III. PROBLEM MOTIVATION AND FORMULATION

A. Motivation

It is desirable to achieve real-time inference execution on edge-computing platforms. This paper mainly focuses on the 3D object detection task, which is of essential importance in autopilot for self-driving cars. However, the existing works on 3D object detection mainly use the powerful GPUs with large memory and computation capacities for inference, which are not available on vehicles due to the cost considerations. It is a challenging task to deploy 3D object detection with real-time inference performance on resource-limited computing devices on self-driving cars.

To satisfy the real-time requirement, we adopt model pruning and network enhancement together with compiler optimizations to accelerate the inference and mitigate the potential mean average precision (mAP) loss. Previous works usually have fixed pruning methods and pruning type for the whole model. However, we find that for the same layer, different pruning types with different pruning ratios have various inference speedup as shown in Figure 1 (a). Thus, different layers may have different best-suited pruning types. Besides, we observe that the layer-wise speed or latency of different kernel sizes under compiler optimization are also different as shown in Figure 1 (b). Moreover, Winograd can speedup the inference although incurring transformation overheads. Thus, the performance of network enhancement techniques needs to be re-evaluated to in terms of transformation overhead, inference speed and mAP. Meanwhile, designing the pruning and network enhancement requires much human expertise and efforts in hyperparameter fine-tuning.

Based on the above observations, we propose to use a compiler-aware unified framework with network enhancement and pruning search to find a unified scheme so that the

enhanced and pruned model can satisfy the mAP and real-time requirements for 3D object detection, thus facilitating the 3D detection deployment on edge devices. We highlight that the framework is based on RL which automatically generates the unified scheme without human assistance by searching the unified search space.

B. Problem Definition

In this problem, we search a unified scheme with network enhancement and pruning, such that the enhanced and pruned model can keep the mean average precision (mAP) as high as possible while satisfying the latency or real-time requirement, that is, the whole inference time should not exceed a threshold. The problem can be formulated as below,

$$\min_s \mathcal{L}_{val}(\hat{\theta}(s)), \quad (1)$$

$$\text{s.t. } \hat{\theta}(s) = \operatorname{argmin}_{\theta} \mathcal{L}_{train}(\theta(s)), \quad (2)$$

$$t(\hat{\theta}(s)) \leq T, \quad (3)$$

where s denotes a unified scheme including a list of enhancement and pruning actions, and $\theta(s)$ denotes the new model parameters following the unified scheme. \mathcal{L}_{train} and \mathcal{L}_{val} represent the training and the validation loss, respectively. $t(\cdot)$ denotes the inference time of the model and T is the real-time or latency requirement for inference. The constraint (2) is the retraining or fine-tuning step after performing the unified scheme to further improve mAP and mitigate the mAP loss. The constraint (3) is the real-time requirement that its inference time after enhancement and pruning should not go beyond a threshold.

C. Unified Search Space

For solving problem (1), we search a unified space to find a unified scheme incorporating the network enhancement and model pruning. For network enhancements, we employ intra-kernel replacement to choose a suitable kernel size and explore the usage of Winograd [31] for inference acceleration. For pruning search, we choose the pruning method, pruning type and pruning ratio separately. We list the choice of the network enhancement and pruning search in Table I and specify them in the following sections.

TABLE I: Unified search space

Network enhancement	Intra-kernel replacement	$\{1 \times 1, 3 \times 3, \text{DW } 3 \times 3 \text{ \& } 1 \times 1\}$
	Winograd	$\{0, 1\}$ ^a
Pruning search	Pruning method	Magnitude pruning [14], [37] ADMM pruning [63], [32]
	Pruning type	Filter pruning [23] Pattern pruning [39] Block pruning
	Pruning ratio	$\{0, 0.3, 0.5, 0.7, 0.8, 0.9\}$

^a 1 and 0 denote using this method or not;

1) *Network Enhancement Space*: The network enhancements include intra-kernel replacement to choose a suitable kernel size and whether to use Winograd [31], [3] for inference acceleration.

a) *Intra-kernel replacement*.: Under compiler optimization, different kernel sizes result in various speedups. Besides, changing kernel size may boost model performance [61]. Thus we consider to search different kernel sizes. As the compiler can achieve higher accelerations on small kernel sizes, we mainly choose between 1×1 , 3×3 , and a cascade of depthwise (DW) 3×3 & 1×1 [24], [49].

b) *Winograd*.: Winograd [31], [3] can reduce the arithmetic complexity of a CONV layer by up to a factor of 4 compared to direct convolution. However, the transformations in Winograd cause certain computational overheads which could degrade the performance improvement. Thus, we explore the usage of Winograd to confirm whether it can improve the inference speed.

2) *Pruning Search Space*: The pruning scheme includes three aspects: pruning method, layer-wise pruning type and pruning ratio. For pruning methods, we search from magnitude pruning [14] and ADMM pruning [63]. Different pruning methods could lead to different pruning locations even with the same pruning type and ratio. For pruning types, we explore the space of filter pruning [23], pattern pruning [39] and block pruning (specified below) for each layer. Besides, in each layer, along with the pruning type, we choose a pruning ratio from $\{0, 0.3, 0.5, 0.7, 0.8, 0.9, \}$, denoting the percentage of pruned weights. 0 means skip pruning.

Note that in previous pruning [63], [23], [39], [19], all the DNN layers usually share the same pruning type under a fixed pruning method, and the layer-wise pruning ratio is manually predefined. However, each layer may have different best-suited pruning types under the compiler optimization due to its unique computation pattern and layer size. Thus, different from the fixed pruning scheme, we use configurable pruning design, which allows each layer to choose its own pruning type and its corresponding pruning ratio, and the whole model to choose a pruning method.

a) *Block pruning*.: As pattern pruning [39] can only be applied to 3×3 CONV layers, we propose block pruning as a more general fine-grained structured pruning type compatible with various CONV kernel sizes. More specifically, the weights of a CONV layer has the shape $c_{in} \times c_{out} \times n \times n$ where c_{in} and c_{out} are the input and output channel numbers respectively for this layer, and n is the kernel size. We first divide the weights into $b_{in} \times b_{out}$ blocks, and each block has the shape $\frac{c_{in}}{b_{in}} \times \frac{c_{out}}{b_{out}} \times n \times n$. So the block division is carried out on the input and output channels instead of the kernels. Next, in block pruning, all of the kernels in the same block share the same pruning patterns, which means we prune the same locations for all kernels in this block. The pruning patterns of different blocks can be different, so the pruned locations of two kernels from two different blocks are not necessarily the same. With block pruning, we can leverage hardware parallelism with compiler optimizations to improve inference speed.

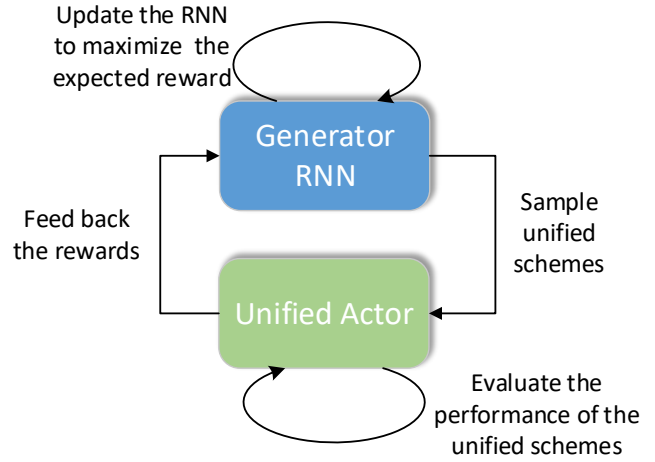


Fig. 2: Unified network enhancement and pruning search framework.

D. Compiler Assistance

To achieve real-time performance on edge devices, we incorporate compiler optimization to accelerate inference. Therefore, we should be able to obtain the inference speed performance of pruned and enhanced models under the given compiler optimizations. More specifically, we build up an automatic code generation framework to incorporate compiler optimizations. The compiler optimizations consist of several components including domain specific language related optimizations, sparse model storage, matrix reorder, etc. [39] to improve the inference speed on edge devices. We show more details in Appendix A. Given a pruned and enhanced model, the framework can dynamically perform compiler-level optimizations to accelerate the inference of each layer in the model based on the pruning type and pruning ratio. The framework supports various pruning types such as filter pruning [23], pattern pruning [39] and block pruning. We demonstrate the superior inference acceleration performance on sparse DNN models in Appendix B. Thus, the framework can provide the speed performance of DNN models with compiler optimizations.

IV. UNIFIED FRAMEWORK WITH RL

In this section, we first describe the framework of the proposed unified network enhancement and pruning search as shown in Figure 2. It has two main functional components: the generator RNN and the unified actor. The generator is implemented by a RNN to generate various unified schemes. After receiving the unified scheme, the unified actor starts to perform the network enhancement and pruning on the original model following the unified scheme. Once finished, its reward (the mAP and speed performance) is sent back to the generator RNN. Then the generator RNN is updated with a policy gradient method to maximize the expected reward of the sampled schemes.

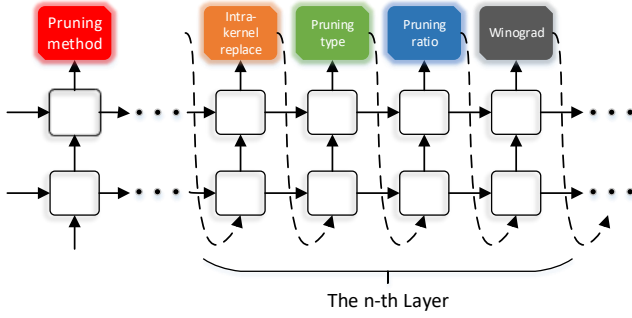


Fig. 3: Unified scheme generation.

A. Setup

Before the generator RNN outputs the unified schemes, we need to initialize the generator RNN and perform some preliminary analysis for the given model. In the 3D object detection with point clouds, we train a PointPillars model [30] as the original starting model. Note that we do not choose other 3D sparse convolution based models such as PV-RCNN [52] or SECOND [59] since the PointPillars model has the best inference speed performance with competitive mAP. For example, when executed on Nvidia high-end GPU, it has inference latency of 20ms, which is at least 2.7 times faster than other models. Besides, other methods are not well supported by compiler optimization. Given the PointPillars model, we first investigate the model architecture and obtain the statistics of the whole model and each layer, including its parameter shapes, number of multiply-accumulate operation (MAC) and so on. This information can help with the compiler optimizations.

B. Generator RNN

1) *Unified Scheme Generation*: In the unified framework, a generator RNN is applied to generate the unified schemes. The generator RNN generates the details of a unified scheme including network enhancement options (intra-kernel replace and Winograd for each layer) and pruning search exploration (pruning method, layer-wise pruning type and its corresponding pruning ratio), as a sequence of tokens shown in Figure 3. Every prediction is carried out with a softmax classifier and then fed into the next time step as input. Once the generator RNN finishes generating a unified scheme, it will be evaluated and its reward is used to train the parameters of the generator RNN, θ_c .

2) *Generator Training*: The list of tokens that the generator RNN predicts represents a list of actions $s_{1:Q}$ for a unified scheme, where Q is the number of total hyperparameters or actions. Following this unified scheme, the processed model achieves a mAP A on the test dataset with an average inference time t on edge platforms. We define the reward function as the following,

$$R = A - \alpha \cdot \max(0, t - T), \quad (4)$$

where T is the real-time requirement for inference and α controls the relative significance of the mAP and inference time. Basically, if the processed model achieves high mAP

Algorithm 1: Unified framework

Input: Original model;
Output: The best unified scheme and pruned model;

- 1 Setup to get statistics of the original model;
- 2 Initialize the parameters of GR¹;
- 3 **for each step do**
- 4 GR samples K unified schemes;
- 5 UA selects B unified schemes with the BO acquisition function from the K schemes;
- 6 **for each selected scheme do**
- 7 UA performs evaluation to obtain the mAP and speed performance;
- 8 UA sends the evaluation performance to GR;
- 9 GR obtains the gradients with rewards;
- 10 GR updates its parameters;
- 11 UA updates the GP of BO with the new observation data;
- 12 Fine-tune the best pruned model to further improve its performance;

¹ GR denotes the generator RNN.

² UA denotes the unified actor.

and its inference time does not exceed the threshold, it will get a high reward. Otherwise if A is small or $t > T$, the reward becomes smaller.

The generator is trained to maximize its expected reward which is non-differentiable. To deal with this, we adopt an empirical approximation of the REINFORCE rule [58] and its gradients can be given by the following,

$$\nabla_{\theta_c} J(\theta_c) = \frac{1}{K} \sum_{k=1}^K \sum_{q=1}^Q \nabla_{\theta_c} \log P(s_q | s_{(q-1):1}; \theta_c) (R_k - b), \quad (5)$$

where $P(s_q | s_{(q-1):1}; \theta_c)$ is the probability of the action s_q in the unified scheme s from the generator RNN θ_c . K is the number of different unified schemes sampled by the generator in one batch. The reward of the k -th unified scheme is R_k . We introduce b as the exponential moving average of the previous reward to reduce the estimate variance. We show the reinforcement training progress in Algorithm 1.

C. Unified Actor with Bayesian Optimization

The main function for the unified actor is to obtain the mAP and speed performance of the K unified schemes from the generator. However, evaluating the scheme performance is expensive as it needs pruning and training the model with certain epochs. Moreover, the search space is large, leading to difficulties for finding a scheme with a good performance. Thus we first use Bayesian optimization (BO) [55], [27], [8] with Weisfeiler-Lehman (WL) kernel [42], [51] to select a subset of unified schemes from the generator. Then we perform actual evaluation for the selected schemes.

1) *BO with WL Kernel*: To accelerate the training process, we propose to use BO to help with the unified actor for reducing the number of actual evaluated schemes. More specifically, given K unified schemes, before we actually evaluate them, BO is first utilized to find B ($B < K$) unified schemes through the acquisition function. The selected B schemes may achieve better performance with high probabilities while the rest $K - B$

schemes are potentially weak. Thus, during evaluation, we only evaluate the selected B unified schemes and obtain their real performance while the rewards of the rest $K - B$ schemes are obtained with the Gaussian process (GP) surrogate model. However, conventional BO cannot be directly employed since the unified schemes can be treated as a directed acyclic graph (DAG). To facilitate this, we use a GP with a WL graph kernel which can naturally deal with the non-continuous graphs.

The WL kernel compares two directed graphs as below,

$$k_{\text{WL}}^H(s, s') = \sum_{h=0}^H w_h k_{\text{base}}(\phi_h(s), \phi_h(s')), \quad (6)$$

where h denotes the WL iteration index and H denotes the maximum iteration level. In the h -th WL iteration, it first collects the graph features $\phi_m(s)$ and $\phi_m(s')$ for two graphs s and s' , and then compares the two graphs with $k_{\text{base}}(\phi_m(s), \phi_m(s'))$. The final WL kernel is the weighted sum of the comparison in each iteration. We employ the dot product as the base kernel k_{base} and w_h are the weights of each WL iteration, which are set to equal following [51]. The details of WL kernel are demonstrated in Appendix C. We adopt the expected improvement [47], [15] as the acquisition function in the work.

2) *Scheme Evaluation*: In the scheme evaluation, for each unified scheme, the unified actor processes the original model following the unified scheme. It first perform the intra-kernel replacement by replacing the kernel with new kernel sizes and finetuning the new model with a few epochs. Then it starts to prune the model. It can perform multiple kinds of pruning method such as ADMM pruning [63] or magnitude pruning [14] with supports for various pruning types and pruning ratios.

After pruning and retraining, we can obtain the mAP of the pruned model. The inference speed of the pruned model can be obtained by the compiler optimization framework with the configuration of Winograd from the scheme as shown in Section III-D. The compiler optimization can be performed in parallel with the finetuning step in the pruning during evaluation.

D. Acceleration Techniques

The unified framework requires to prune the model multiple times with different pruning schemes to train the generator RNN until convergence. It could be time-consuming to collect the large pruning performance data. To accelerate the generator training, we employ several acceleration techniques including parallel updating and early stop as demonstrated in Appendix D with details.

V. EXPERIMENTAL RESULTS

A. Experiment setting

All experiments are conducted with the KITTI object detection benchmark dataset [16], which consists of samples with both lidar point clouds and images. We follow the standard convention [64] of only using lidar points, but compare with fusion methods that use both lidar and images. We train a

TABLE II: Comparison with the original model

	PointPillars (0.16)	Ours (0.16)	PointPillars (0.24)	Ours (0.24)
Parameter #	5.8M	1.1M	5.8M	0.8M
Computation # (MACs)	60G	10.7G	28G	3.9G
Server GPU speed (ms)	25	24	20	18
Mobile GPU speed (ms)	542	189	257	97
Car 3d detection AP	Easy	84.69	85.50	84.05
	Moderate	75.11	76.58	74.99
	Hard	69.53	70.58	68.30

PointPillars for cars use a pillar resolution of 0.24 m with 12000 as the max number of pillars and 100 as the max number of points per pillar. More results for pedestrians and cyclists are shown in Appendix E. During inference, we apply axis aligned non maximum suppression (NMS) with an overlap threshold of 0.7 intersection-over-union (IoU) following the official KITTI protocol.

The generator RNN is a two-layer LSTM with 49 hidden units on each layer. Its weights are initialized uniformly between -0.1 and 0.1. The ADAM optimizer [26] is employed with a learning rate of 0.0005. For the parallel training, we use 50 GPUs to concurrently evaluate the unified schemes. The generator training takes about 10 days. During the evaluation, for each unified scheme, we first perform intra-kernel replacement and fine-tuning the model with 5 epochs. Then we start to prune the model. For ADMM pruning, we prune with 5 epochs and fine-tune the pruned model with 10 epochs. For magnitude pruning, we first prune the model according to weight magnitudes and then fine-tune the model with 10 epochs. Note that we start from a well-trained model and thus it does not need too many epochs to obtain competitive results with network enhancement and pruning. We use the ADAM Optimizer [26] with a learning rate of 0.0002, weight decay of 1e-4 and momentum of 0.8. More training hyperparameter settings are shown in Appendix F.

B. Comparison with the Original Model

The original unpruned model is based on PointPillars [53]. We compare the performance of the original model and the model found by our method shown in Table II. We try two pillar grid sizes 0.16×0.16 and 0.24×0.24 (large grid sizes means small input size for the model) and their real-time requirement are set to 200ms and 100ms respectively. We can make the following observations. (1) Although the parameter numbers are not large, the computation numbers (MACs) are relatively large due to the tremendous CONV operations, leading to difficulties for achieving real-time on mobile. (2) Small input size results in obvious computation reduction (60G v.s. 28G for original PointPillars model). (3) As the server GPU (GTX 1080Ti) is far more powerful than the mobile (Samsung Galaxy S20 phone) GPU, the speed on mobile is much slower than that on server GPU (e.g. 542ms v.s. 25ms), thus it is more challenging to achieve real-time on mobile. (4) Although the parameter and computation number are reduced significantly by pruning, the speed on powerful

TABLE III: Comparison of 3D detection methods

Detection methods	Modality	Server GPU speed (ms)	Mobile GPU speed (ms)	Car 3D detection			Car BEV detection		
				Easy	Moderate	Hard	Easy	Moderate	Hard
F-PointNet [46]	R+L ^a	170	-	82.13	69.22	60.78	90.58	84.73	75.12
AVOD-FPN [28]		100	-	82.77	71.94	66.31	90.64	84.37	80.04
UberATG-MMF [33]		80	-	86.81	76.75	68.41	89.49	87.47	79.10
Fast Point R-CNN [9]	L	65	-	85.39	77.46	70.21	89.97	87.08	80.40
STD [60]		80	-	86.61	77.63	76.06	89.66	87.76	86.89
SECOND [59]		50	-	83.34	72.55	65.82	89.39	83.77	78.59
Point-GNN [53]		643	-	87.25	78.34	72.29	92.04	88.20	81.97
Ours		18	97	85.20	75.57	68.37	90.02	86.79	80.80

^a 'L' and 'R' represent LiDAR and RGB images respectively;

server GPUs does not naturally get obvious improvements (e.g. 25ms v.s. 24 ms) without further optimizations. (5) Different from the server speed, with compiler optimization, the mobile speed can be improved significantly after pruning (with about $2.7\times$ speedup). (6) The detection performance of the our models are better than the original model indicating that there may be certain overfitting or redundancy in the original model, resulting in the lower performance.

Based on the above observations, we mainly focus on the configuration with grid size 0.24×0.24 . We demonstrate that the proposed method can achieve real-time inference (97ms) on mobile devices (Samsung Galaxy S20 phone) with state-of-the-art detection performance. Although there are some other DNN inference acceleration frameworks such as Tensorflow-Lite [1], TVM [7] and MNN [2], we are the first to support real-time 3D object detection on mobile GPUs.

C. Comparison of 3D Detection Methods

We show the performance of the model obtained through the proposed method compared with state-of-the-art 3D object detection methods as shown in Table III. We obtain the statistics of other methods by following their released code or model with the default setting. The server GPU inference time is obtained on GTX 1080Ti and the mobile GPU speed is based on the Samsung Galaxy S20 phone.

We can observe that the proposed method can achieve competitive 3D detection performance with the fastest speed. On server GPU, it only needs 18ms to process one input sample during inference on average. Compared with other methods not based on PointPillars, the speed are at least $2.7\times$ faster with competitive detection performance. On mobile GPU, our method achieves an average 97ms inference speed, satisfying the real-time requirement, while we are not able to perform compiler optimization and obtain their mobile speed for most of the other 3D object detection methods. The reason is that their proposed various special layers or structures to deal with the sparse data are currently not supported by the compiler optimization. For example, the 3D sparse convolutions [18] which are adopted by many 3D detection works uses highly irregular data and computation patterns such as Hash table, leading to difficulties of compiler optimizations to improve computation parallelism.

TABLE IV: Comparison of various pruning methods

Pruning methods	server GPU Speed (ms)	mobile GPU Speed (ms)	Car 3D detection		
			Easy	Moderate	Hard
Original	20	257	84.05	74.99	68.30
Filter [23]	18	81	81.54	68.10	65.90
Pattern [39]	19	111	80.97	73.77	68.05
Block	20	143	80.88	72.98	67.85
Ours	18	97	85.20	75.57	68.37

D. Comparison of Pruning Frameworks

We compare the performance of the proposed method with other pruning types under the ADMM pruning framework [63] as shown in Table IV. All of these methods start from the same PointPillars model. Their pruning ratio are set to the same with the overall pruning ratio of our pruned model (86%). As observed, the proposed method can achieve the best detection performance compared with other methods where all the layers share the same pruning type, demonstrating the advantages of using flexible pruning types for each layer. Besides, with compiler optimization, filter pruning is the fastest but suffers from obvious detection performance degradation. The proposed method can process one lidar image within 97ms on average with the highest precision, demonstrating the superior performance of the proposed method to achieve real-time inference on mobile with state-of-the-art detection performance.

E. Ablation Study

We explore the effects of various pillar grid sizes and show the performance in Appendix G. Besides, we test the case with pruning search only instead of unifying network enhancement and pruning search. Under the same configuration, pruning search only can achieve a mAP of 74.89% with an average inference time of 108ms. Compared with the unified framework with 76.38% mAP and 97ms inference, we can see that incorporating network enhancement can further improve the detection and speed performance. Moreover, As we increase the real-time requirement from 100ms to 90ms, the proposed method achieves a mAP of 74.15% with an average 89ms speed, demonstrating that the method prune

the model harder to improve speed, thus incurring detection performance degradation. More details are shown in Appendix G.

VI. CONCLUSION

We propose a unified framework incorporating network enhancement and pruning search with reinforcement learning to achieve real-time inference on mobile for 3D object detection. The compiler-aware framework includes the detection and speed performance during the optimization and employ BO to accelerate the training. The experimental results show that it can satisfy the real-time requirement on mobile with competitive detection performance compared with state-of-the-art 3D detection works.

REFERENCES

- [1] <https://www.tensorflow.org/mobile/tflite/>. 1, 2, 7
- [2] <https://github.com/alibaba/MNN>. 1, 2, 7
- [3] Barbara Barabasz and David Gregg. Winograd convolution for dnns: Beyond linear polynomials. In Mario Alviano, Gianluigi Greco, and Francesco Scardello, editors, *AI*IA 2019 – Advances in Artificial Intelligence*, pages 307–320, Cham, 2019. Springer International Publishing. 1, 2, 3, 4
- [4] Alexey Bochkovskiy, Chien-Yao Wang, and Hong-Yuan Mark Liao. Yolov4: Optimal speed and accuracy of object detection. *arXiv preprint arXiv:2004.10934*, 2020. 1
- [5] Han Cai, Tianyao Chen, Weinan Zhang, Yong Yu, and Jun Wang. Efficient architecture search by network transformation. *AAAI*, 2018. 2
- [6] Han Cai, Ligeng Zhu, and Song Han. Proxylessnas: Direct neural architecture search on target task and hardware. *arXiv preprint arXiv:1812.00332*, 2018. 3
- [7] Tianqi Chen, Thierry Moreau, Ziheng Jiang, Lianmin Zheng, Eddie Yan, Meghan Cowan, Haichen Shen, Leyuan Wang, Yuwei Hu, Luis Ceze, Carlos Guestrin, and Arvind Krishnamurthy. Tvm: An automated end-to-end optimizing compiler for deep learning. OSDI’18, page 579–594, USA, 2018. USENIX Association. 1, 2, 7, 10
- [8] Yutian Chen, Aja Huang, Ziyu Wang, Ioannis Antonoglou, Julian Schrittwieser, David Silver, and Nando de Freitas. Bayesian optimization in alphago. *arXiv preprint arXiv:1812.06855*, 2018. 5
- [9] Yilun Chen, Shu Liu, Xiaoyong Shen, and Jiaya Jia. Fast point r-cnn. In *Proceedings of the IEEE International Conference on Computer Vision*, pages 9775–9784, 2019. 7
- [10] Martin Cunneen, Martin Mullins, and Finbarr Murphy. Autonomous vehicles and embedded artificial intelligence: The challenges of framing machine driving decisions. *Applied Artificial Intelligence*, 33(8):706–731, 2019. 1
- [11] Jeffrey Dean, Greg Corrado, Rajat Monga, Kai Chen, Matthieu Devin, Mark Mao, Marc’auelio Ranzato, Andrew Senior, Paul Tucker, Ke Yang, et al. Large scale distributed deep networks. In *Advances in neural information processing systems*, pages 1223–1231, 2012. 11
- [12] Thomas Elsken, Jan Hendrik Metzen, and Frank Hutter. Neural architecture search: A survey. *arXiv preprint arXiv:1808.05377*, 2018. 2
- [13] Ben Fielding and Li Zhang. Evolving image classification architectures with enhanced particle swarm optimisation. *IEEE Access*, 6:68560–68575, 2018. 3
- [14] Jonathan Frankle and Michael Carbin. The lottery ticket hypothesis: Finding sparse, trainable neural networks. *ICLR*, 2018. 1, 2, 3, 4, 6
- [15] PI Frazier. A tutorial on bayesian optimization. arxiv 2018. *arXiv preprint arXiv:1807.02811*. 6
- [16] Andreas Geiger, Philip Lenz, and Raquel Urtasun. Are we ready for autonomous driving? the kitti vision benchmark suite. In *Conference on Computer Vision and Pattern Recognition (CVPR)*, 2012. 6, 12
- [17] Ian Goodfellow, Yoshua Bengio, Aaron Courville, and Yoshua Bengio. *Deep learning*, volume 1. MIT press Cambridge, 2016. 1
- [18] Ben Graham. Sparse 3d convolutional neural networks. *arXiv preprint arXiv:1505.02890*, 2015. 7
- [19] Yiwen Guo, Anbang Yao, and Yurong Chen. Dynamic network surgery for efficient dnns. In *Advances in neural information processing systems (NeurIPS)*, pages 1379–1387, 2016. 1, 2, 4
- [20] Song Han, Jeff Pool, John Tran, and William Dally. Learning both weights and connections for efficient neural network. In *Advances in neural information processing systems (NeurIPS)*, pages 1135–1143, 2015. 2
- [21] X He, K Zhao, and X Chu. Auttml: A survey of the state-of-the-art. arxiv 2019. *arXiv preprint arXiv:1908.00709*, 1908. 1
- [22] Yihui He, Ji Lin, Zhijian Liu, Hanrui Wang, Li-Jia Li, and Song Han. Amc: Auttml for model compression and acceleration on mobile devices. In *Proceedings of the European Conference on Computer Vision (ECCV)*, pages 784–800, 2018. 1, 2
- [23] Yang He, Ping Liu, Ziwei Wang, Zhilan Hu, and Yi Yang. Filter pruning via geometric median for deep convolutional neural networks acceleration. In *Proceedings of the IEEE Conference on Computer Vision and Pattern Recognition (CVPR)*, pages 4340–4349, 2019. 1, 2, 3, 4, 7
- [24] Andrew Howard, Menglong Zhu, Bo Chen, Dmitry Kalenichenko, Weijun Wang, Tobias Weyand, Marco Andreetto, and Hartwig Adam. Mobilenets: Efficient convolutional neural networks for mobile vision applications. *arXiv:1704.04861*, 2017. 4
- [25] Kirthevasan Kandasamy, Willie Neiswanger, Jeff Schneider, Barnabas Poczos, and Eric P Xing. Neural architecture search with bayesian optimisation and optimal transport. In *Advances in neural information processing systems*, pages 2016–2025, 2018. 1
- [26] Diederik P Kingma and J Adam Ba. A method for stochastic optimization. arxiv 2014. *arXiv preprint arXiv:1412.6980*, 434, 2019. 6, 12
- [27] Aaron Klein, Stefan Falkner, Simon Bartels, Philipp Hennig, and Frank Hutter. Fast bayesian optimization of machine learning hyperparameters on large datasets. In *Artificial Intelligence and Statistics*, pages 528–536. PMLR, 2017. 5
- [28] Jason Ku, Melissa Mozifian, Jungwook Lee, Ali Harakeh, and Steven L Waslander. Joint 3d proposal generation and object detection from view aggregation. In *2018 IEEE/RSSJ International Conference on Intelligent Robots and Systems (IROS)*, pages 1–8. IEEE, 2018. 7, 12
- [29] Nicholas D Lane, Sourav Bhattacharya, Petko Georgiev, Claudio Forlivesi, and Fahim Kawsar. An early resource characterization of deep learning on wearables, smartphones and Internet-of-Things devices. In *Proceedings of the 2015 International Workshop on Internet of Things towards Applications*, pages 7–12. IEEE, 2015. 1
- [30] Alex H Lang, Sourabh Vora, Holger Caesar, Lubing Zhou, Jiong Yang, and Oscar Beijbom. Pointpillars: Fast encoders for object detection from point clouds. In *Proceedings of the IEEE Conference on Computer Vision and Pattern Recognition*, pages 12697–12705, 2019. 5, 12
- [31] Andrew Lavin and Scott Gray. Fast algorithms for convolutional neural networks. In *Proceedings of the IEEE Conference on Computer Vision and Pattern Recognition*, pages 4013–4021, 2016. 1, 2, 3, 4
- [32] Tuanhui Li, Baoyuan Wu, Yujiu Yang, Yanbo Fan, Yong Zhang, and Wei Liu. Compressing convolutional neural networks via factorized convolutional filters. In *Proceedings of the IEEE Conference on Computer Vision and Pattern Recognition (CVPR)*, pages 3977–3986, 2019. 2, 3
- [33] Ming Liang, Bin Yang, Yun Chen, Rui Hu, and Raquel Urtasun. Multi-task multi-sensor fusion for 3d object detection. In *Proceedings of the IEEE Conference on Computer Vision and Pattern Recognition*, pages 7345–7353, 2019. 7, 12
- [34] Chenxi Liu, Barret Zoph, Maxim Neumann, Jonathon Shlens, Wei Hua, Li-Jia Li, Li Fei-Fei, Alan Yuille, Jonathan Huang, and Kevin Murphy. Progressive neural architecture search. In *Proceedings of the European Conference on Computer Vision (ECCV)*, pages 19–34, 2018. 2, 3
- [35] Hanxiao Liu, Karen Simonyan, and Yiming Yang. Darts: Differentiable architecture search. *arXiv preprint arXiv:1806.09055*, 2018. 1, 2, 3
- [36] Ning Liu, Xiaolong Ma, Zhiyuan Xu, Yanzhi Wang, Jian Tang, and Jieping Ye. Autocompress: An automatic dnn structured pruning framework for ultra-high compression rates. In *AAAI*, 2020. 2
- [37] Zhuang Liu, Mingjie Sun, Tinghui Zhou, Gao Huang, and Trevor Darrell. Rethinking the value of network pruning. *arXiv preprint arXiv:1810.05270*, 2018. 2, 3
- [38] Renqian Luo, Fei Tian, Tao Qin, Enhong Chen, and Tie-Yan Liu. Neural architecture optimization. In *Advances in neural information processing systems*, pages 7816–7827, 2018. 2
- [39] Xiaolong Ma, Fu-Ming Guo, Wei Niu, Xue Lin, Jian Tang, Kaisheng Ma, Bin Ren, and Yanzhi Wang. Pconv: The missing but desirable sparsity in dnn weight pruning for real-time execution on mobile devices. In *Thirty-Four AAAI Conference on Artificial Intelligence*, 2020. 1, 2, 3, 4, 7
- [40] Xiaolong Ma, Geng Yuan, Sheng Lin, Caiwen Ding, Fuxun Yu, Tao Liu, Wujie Wen, Xiang Chen, and Yanzhi Wang. Tiny but accurate:

- A pruned, quantized and optimized memristor crossbar framework for ultra efficient dnn implementation. In *ASP-DAC*, 2020. 2
- [41] Chuhan Min, Aosen Wang, Yiran Chen, Wenyao Xu, and Xin Chen. 2pfpce: Two-phase filter pruning based on conditional entropy. *arXiv preprint arXiv:1809.02220*, 2018. 2
- [42] Christopher Morris, Kristian Kersting, and Petra Mutzel. Globalized weisfeiler-lehman graph kernels: Global-local feature maps of graphs. In *2017 IEEE International Conference on Data Mining (ICDM)*, pages 327–336. IEEE, 2017. 5
- [43] Wei Niu, Xiaolong Ma, Sheng Lin, Shihao Wang, Xuehai Qian, Xue Lin, Yanzhi Wang, and Bin Ren. Patdnn: Achieving real-time dnn execution on mobile devices with pattern-based weight pruning. *arXiv preprint arXiv:2001.00138*, 2020. 2
- [44] Adam Paszke, Sam Gross, Francisco Massa, Adam Lerer, et al. Pytorch: An imperative style, high-performance deep learning library. In *NeurIPS*, 2019. 1
- [45] Damian Philipp, Frank Durr, and Kurt Rothermel. A sensor network abstraction for flexible public sensing systems. In *2011 IEEE Eighth International Conference on Mobile Ad-Hoc and Sensor Systems (IEEE MASS 2011)*, pages 460–469. IEEE, 2011. 1
- [46] Charles R Qi, Wei Liu, Chenxia Wu, Hao Su, and Leonidas J Guibas. Frustum pointnets for 3d object detection from rgb-d data. In *Proceedings of the IEEE conference on computer vision and pattern recognition*, pages 918–927, 2018. 7, 12
- [47] Chao Qin, Diego Klabjan, and Daniel Russo. Improving the expected improvement algorithm. In *Advances in Neural Information Processing Systems*, pages 5381–5391, 2017. 6
- [48] Binxin Ru, Xingchen Wan, Xiaowen Dong, and Michael Osborne. Neural architecture search using bayesian optimisation with weisfeiler-lehman kernel. *arXiv preprint arXiv:2006.07556*, 2020. 1
- [49] Mark Sandler, Andrew Howard, Menglong Zhu, Andrey Zhmoginov, and Liang-Chieh Chen. Mobilenetv2: Inverted residuals and linear bottlenecks. In *Proceedings of the IEEE Conference on Computer Vision and Pattern Recognition*, pages 4510–4520, 2018. 4
- [50] Fabrizio Sebastiani. Machine learning in automated text categorization. *ACM computing surveys (CSUR)*, 34(1):1–47, 2002. 1
- [51] Nino Shervashidze, Pascal Schweitzer, Erik Jan van Leeuwen, Kurt Mehlhorn, and Karsten M. Borgwardt. Weisfeiler-lehman graph kernels. *Journal of Machine Learning Research*, 12(77):2539–2561, 2011. 5, 6
- [52] Shaoshuai Shi, Chaoxu Guo, Li Jiang, Zhe Wang, Jianping Shi, Xiaogang Wang, and Hongsheng Li. Pv-rcnn: Point-voxel feature set abstraction for 3d object detection. In *Proceedings of the IEEE/CVF Conference on Computer Vision and Pattern Recognition*, pages 10529–10538, 2020. 5
- [53] Weijing Shi and Raj Rajkumar. Point-gnn: Graph neural network for 3d object detection in a point cloud. In *Proceedings of the IEEE/CVF Conference on Computer Vision and Pattern Recognition*, pages 1711–1719, 2020. 6, 7, 12
- [54] Karen Simonyan and Andrew Zisserman. Very deep convolutional networks for large-scale image recognition. *arXiv preprint arXiv:1409.1556*, 2014. 1
- [55] Jasper Snoek, Hugo Larochelle, and Ryan P Adams. Practical bayesian optimization of machine learning algorithms. In *Advances in neural information processing systems*, pages 2951–2959, 2012. 5
- [56] Bin Wang, Yanan Sun, Bing Xue, and Mengjie Zhang. Evolving deep neural networks by multi-objective particle swarm optimization for image classification. In *Proceedings of the Genetic and Evolutionary Computation Conference*, pages 490–498, 2019. 3
- [57] Wei Wen, Chunpeng Wu, Yandan Wang, Yiran Chen, and Hai Li. Learning structured sparsity in deep neural networks. In *Advances in neural information processing systems (NeurIPS)*, pages 2074–2082, 2016. 1, 2
- [58] Ronald J Williams. Simple statistical gradient-following algorithms for connectionist reinforcement learning. *Machine learning*, 8(3-4):229–256, 1992. 5
- [59] Yan Yan, Yuxing Mao, and Bo Li. Second: Sparsely embedded convolutional detection. *Sensors*, 18(10):3337, 2018. 5, 7, 12
- [60] Zetong Yang, Yanan Sun, Shu Liu, Xiaoyong Shen, and Jiaya Jia. Std: Sparse-to-dense 3d object detector for point cloud. In *Proceedings of the IEEE International Conference on Computer Vision*, pages 1951–1960, 2019. 7
- [61] Jiahui Yu, Yuchen Fan, Jianchao Yang, Ning Xu, Xinchao Wang, and Thomas S Huang. Wide activation for efficient and accurate image super-resolution. *arXiv preprint arXiv:1808.08718*, 2018. 2, 4, 10
- [62] Sergey Zagoruyko and Nikos Komodakis. Wide residual networks. *arXiv preprint arXiv:1605.07146*, 2016. 2
- [63] Tianyun Zhang, Shaokai Ye, Yipeng Zhang, Yanzhi Wang, and Makan Fardad. Systematic weight pruning of dnns using alternating direction method of multipliers. *arXiv preprint arXiv:1802.05747*, 2018. 1, 2, 3, 4, 6, 7
- [64] Yin Zhou and Oncel Tuzel. Voxnet: End-to-end learning for point cloud based 3d object detection. In *Proceedings of the IEEE Conference on Computer Vision and Pattern Recognition*, pages 4490–4499, 2018. 6, 12
- [65] Xiaotian Zhu, Wengang Zhou, and Houqiang Li. Improving deep neural network sparsity through decorrelation regularization. In *IJCAI*, 2018. 2
- [66] Zhuangwei Zhuang, Mingkui Tan, Bohan Zhuang, Jing Liu, Yong Guo, Qingyao Wu, Junzhou Huang, and Jinhui Zhu. Discrimination-aware channel pruning for deep neural networks. In *Advances in Neural Information Processing Systems (NeurIPS)*, pages 875–886, 2018. 2
- [67] Barret Zoph and Quoc V. Le. Neural architecture search with reinforcement learning. In *International Conference on Learning Representations (ICLR)*, 2017. 1, 2, 3

APPENDIX
APPENDIX A
COMPILER OPTIMIZATION DETAILS

Compiler optimization can support all kinds of pruning types and pruning ratios. It can support filter pruning and pattern pruning originally. For block pruning, as all filters in each block share the same pruning patterns, the compiler can skip accessing the same input data corresponding to the pruned weights, thus reducing the memory access pressure among these filters. Besides the memory access, for the computation, since the pruned locations are the same among the filters in each block, they have the same computation indices, which is beneficial for computation parallelism without computation divergence within each block. So block pruning can be implemented more efficiently for computation-intensive CONV layers.

The compiler optimization consists of the following components in details.

a) DSL related optimization.: There are multiple kinds of operators with various computation patterns in the DNN models. We use a new domain specific language (DSL) to represent each DNN model. In this DSL, each layer is represented by a new layer-wised representation (LR). This DSL can show the computation graph within the model. Based on this DSL, we can further utilize some computational graph transformation optimizations. For example, a combination of Convolution layer/Depthwise Convolution layer and BatchNorm layer can be fused into one layer to reduce the data movement and access, thus increasing the instruction level parallelism.

Layer fusion is a common technique in DSL optimization to fuse the computation operators in computation graph. With layer fusion, we can reduce the operator number, and avoid saving the parameters of fused operators and their intermediate computation results. We identify the operators which can be fused based on the computation laws such as associative property and distributive property, and the data access patterns. But as the number of operator combinations is huge in the computation graph, we constrain the search of the potential operator fusion by considering whether the fusion can enlarge the overall computation for CPU/GPU utilization improvement and reduce the memory access for memory efficiency.

b) Sparse model storage.: To further improve data locality, we use a more compact format to store the sparse weights of the model compared with the well-known CSR. Basically, we try our best to avoid storing zero-weights in the model with a high compression rate. This is achieved though removing redundant indices from the structured pruning. The sparse model storage can save the scarce memory-bandwidth of mobile devices.

c) Matrix reorder.: Although structured pruning can transform model kernel matrices into small blocks with various pruning patterns, there are still some well-know challenges for sparse matrix multiplications, such as the heavy load imbalance among each thread, and irregular memory accesses. To deal with these challenges, we adopt a matrix reorder method

by leveraging the structure information from the structured pruning. Take the column pruning as example where the whole columns are pruned. As the whole columns are removed, a certain degree of regularity appears since the rest weights are stored in unpruned columns. Based on this, matrix reorder first rearranges the rows with the same or similar patterns together, i.e., reorders the rows. Then, matrix reorder makes the weights in the column direction (e.g., kernels in CNN) more compact.

d) Parameter auto-tuning.: During the compiler optimization, there are many parameters related to the computation, such as data placement on GPU memory, loop unrolling factors, matrix tiling sizes, etc. To find the best configuration of the parameters, the compiler adopts an auto-tuning process similar to other acceleration frameworks such as TVM [7]. More specifically, a genetic algorithm is employed to explore the parameter space. Besides, the explore efficiency can be improved by increasing the population number in each generation to improve the exploration parallelism.

APPENDIX B
COMPILER OPTIMIZATION PERFORMANCE

We demonstrate the efficacy of compiler optimization through three interesting and important DNN applications, style transfer, DNN coloring, and super resolution. The style transfer model is trained on Microsoft COCO dataset and employs a generative network. DNN coloring can convert gray images into colorful images. It trains on the Places scene dataset to obtain a novel architecture that can jointly extract and fuse global and local features to perform the final colorization. The super resolution can convert low resolution images into images with high resolutions. It is trained on the DIV2K dataset and mainly uses residual blocks with wider activation and linear low-rank convolution [61]. With structured pruning and compiler optimization, we implement the models on a Samsung Galaxy S10 mobile phone. We show the average inference time of three applications on mobile device in Table A1. We can observe that for the inference speed, compared with the unpruned model, structured pruning and compiler optimization can achieve speedups of 4.2 \times , 3.6 \times , and 3.7 \times for style transfer, coloring and super resolution, respectively. Without compiler optimization, the pruning model can be faster than the unpruned model. However, their inference time are still a bit longer than the real-time requirement. For example, the super resolution takes about 192ms without compiler optimization. With compiler optimization, we can observe that their inference speeds are further improved with a ratio of at least 2 \times . It largely reduces the inference time (e.g., from 178ms to 67ms for style transfer), satisfying the real-time requirement. We note that all inference can complete within 75 ms, showing the possibility of achieving real-time executions of complex DNN applications on mobile. We demonstrate that compiler optimization can further improve the speed with significant acceleration performance.

Inference time (ms)	Style	coloring	Super resolution
Unpruned	283	137	269
Pruning	178	85	192
Pruning + compiler	67	38	73

TABLE A1: Average Inference Time on the Mobile Device

APPENDIX C WL KERNEL

We illustrate the WL kernel in Fig. A1. As shown in the figure, at initialization, there are two pruning proposals A and B with features of $m = 0$. At step 1, WL kernel collects the next label of each node. For example, for proposal A, the next node of 0 is 1, so we put the information of the next node into the original node and obtain (0,1). At step 2, it re-encodes or re-labels the new nodes incorporating their neighbour information. For example, (0,1) is relabeled as 5. At step 3, it obtains a new graph with features at $m = 1$. At step 4, WL kernel compares the histogram on both $m = 0$ and $m = 1$ features. The histogram is the number of each node in the graph. The iteration repeats until $m = M$.

APPENDIX D ACCELERATION TECHNIQUES

We adopt parallel updates, early stopping and parallel compiler optimization to accelerate the scheme evaluation.

a) *Parallel updates.*: As pruning a DNN model can take hours, a distributed pruning and asynchronous parameter updating method is adopted in order to speed up the learning of the controller [11]. More specifically, a parameter-server scheme is created to store the shared parameters of the generator RNN replicas. Each generator replica samples B different unified schemes which are evaluated in parallel. When the evaluation finishes, their performance are recorded and the generator can compute gradients. The gradients are then sent back to the parameter server such that all the generator replicas can be updated.

b) *Early stopping.*: For each pruning scheme, the pruning usually have two phases: pruning phase and fine-tuning phase. The pruning phase focuses on finding out what weights should be pruned in each layer and the fine-tuning phase tries to improve the mAP problem while keeping the pruned weights zero. In previous works, it normally costs a lot of training epochs for both phases to get the best pruning performance. However, in our work, we use early stopping strategy to reduce the number of training epochs in each pruning implementation. The training set is split and 10% training data are formulated as a validation set which are never used for training. The loss on the validation set after each training epoch is monitored and we stop training when the monitored validation loss does not get improved for 3 epochs.

c) *Parallel compiler optimization.*: The code generation framework with compiler optimization is adopted to actually measure the inference speed on mobile devices for more accurate speed measurement. The code generation framework supports all kinds of pruning types with the ability to

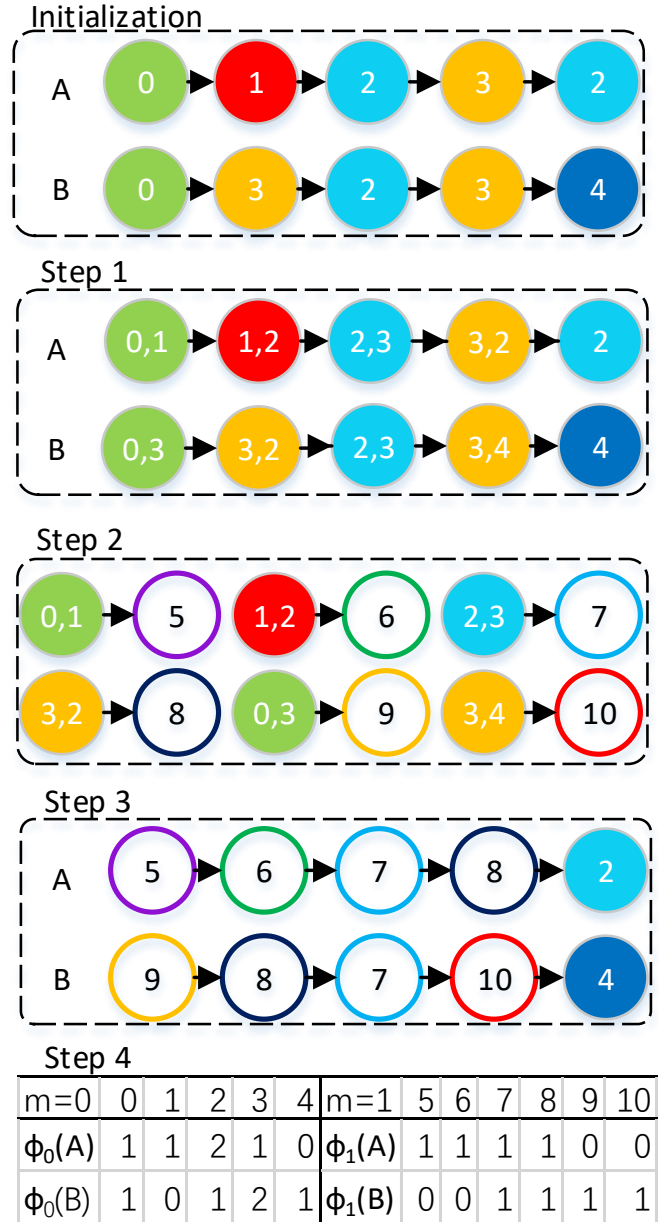


Fig. A1: WL kernel illustration. At initialization, there are two pruning proposals with features at $m = 0$. At step 1, WL kernel collects the next labels of each node. At step 2, it re-encodes or re-labels the new nodes incorporating their neighbour information. At step 3, it obtains a new graph with features at $m = 1$. At step 4, WL kernel compares the histogram on both $m = 0$ and $m = 1$ features. The iteration repeats until $m = M$.

dynamically auto-switch between these pruning types. The speed measurement with compiler optimization usually takes hours. However, it can be performed in parallel with the mAP evaluation step in the actor and does not incur extra time cost. Note that to measure the speed, we do not need the best pruned and well-trained model weights. As long

TABLE A2: Comparison of 3D detection methods

Detection methods	Modality	Server GPU speed (ms)	Mobile GPU speed (ms)	Pedestrian 3D detection			Cyclist 3D detection		
				Easy	Moderate	Hard	Easy	Moderate	Hard
F-PointNet [46]	R+L ^a	170	-	51.21	44.89	40.23	71.96	56.77	50.39
AVOD-FPN [28]		100	-	50.80	42.81	40.88	64.00	52.18	46.61
UberATG-MMF [33]		80	-	-	-	-	-	-	-
PointPillars [30]	L	20	260	52.08	43.53	41.49	75.78	59.07	52.92
SECOND [59]		50	-	51.07	42.56	37.29	70.51	53.85	46.90
Point-GNN [53]		643	-	51.92	43.77	40.14	78.60	63.48	57.08
Ours		18	97	52.33	43.68	41.52	76.09	59.31	53.56

^a 'L' and 'R' represent LiDAR and RGB images respectively;

as the pruned localizations are determined, we can start the speed measurement with compiler optimization while in the meantime the pruned model can be retrained to improve its mAP during evaluation.

APPENDIX E

PERFORMANCE FOR PEDESTRIANS AND CYCLISTS

We show the performance of pedestrians and cyclists in Tab. A2. We can observe that the proposed method can achieve real-time inference on mobile devices with state-of-the-art detection performance. As the server GPU (GTX 1080Ti) is more powerful than the mobile GPU (GPU on Samsung Galaxy S20 phone), the inference speed on server GPU is faster than that on mobile GPU. Besides, since other 3D detection methods use various specific layers and structures, such as sparse 3D CONV layers, leading to highly irregular memory and computation pattern, currently these methods are not supported by the compiler optimization. Moreover, it is also challenging to support these methods with compiler optimization as the irregular patterns are hard to optimize. Although there are some methods with high mAP such as Point-GNN [53], they usually take much longer time (e.g. 643ms for Point-GNN) to process one LiDAR image on average on server GPUs. It is even harder to implement them on mobile GPUs considering the computation resource gap. Although the PointPillars [30] is the fastest on server GPUs, it still takes about 260ms on mobile GPU, which can hardly satisfy the real-time requirement. However, with our proposed method, we can use only 97ms to process one LiDAR image on mobile GPUs, achieving real-time inference on mobile.

APPENDIX F

EXPERIMENTAL SETTING DETAILS

All experiments are conducted with the KITTI object detection benchmark dataset [16], which consists of samples with both lidar point clouds and images. We follow the standard convention [64] of only using lidar points. The dataset is originally divided into 7481 training and 7518 testing samples. For experimental studies we split the official training into 3712 training samples and 3769 validation samples. We train a PointPillars model for cars use a pillar resolution of 0.24m with 12000 as the max number of pillars and 100 as the max

TABLE A3: Comparison of different grid sizes

Pruning methods	server GPU Speed (ms)	mobile GPU Speed (ms)	Car 3D detection		
			Easy	Moderate	Hard
PointPillars [30] (0.16)	25	542	84.67	75.11	69.53
PointPillars [30] (0.24)	20	257	84.05	74.99	68.30
PointPillars [30] (0.32)	18	223	80.81	69.48	67.19
Ours (0.16)	24	189	85.50	76.58	70.58
Ours (0.24)	18	97	85.20	75.57	68.37
Ours (0.32)	17	85	80.98	70.14	67.37

number of points per pillar. During inference, we apply axis aligned non maximum suppression (NMS) with an overlap threshold of 0.7 intersection-over-union (IoU) following the official KITTI protocol.

The generator RNN is a two-layer LSTM with 49 hidden units on each layer. Its weights are initialized uniformly between -0.1 and 0.1. The ADAM optimizer [26] is employed with a learning rate of 0.0005. For the parallel training, we use 50 GPUs to concurrently evaluate the unified schemes. The generator training takes about 10 days.

During the evaluation, for each unified scheme, we first perform intra-kernel replacement and fine-tuning the model with 5 epochs. Then we start to prune the model. For ADMM pruning, we prune with 5 epochs and fine-tune the pruned model with 10 epochs. For magnitude pruning, we first prune the model according to weight magnitudes and then fine-tune the model with 10 epochs. Note that we start from a well-trained model and thus it does not need too many epochs to obtain competitive results with network enhancement and pruning. We use the ADAM Optimizer [26] with a learning rate of 0.0002, weight decay of 1e-4 and momentum of 0.8.

For the reward function (Eq. (4)), we set α to 0.01 and the inference time and threshold are measured in millisecond to incur large penalty so that the speed requirement is more significant than the mAP improvement.

For the Bayesian optimization, we set the Bayesian batch size $B = 10$ (i.e., we select unified schemes with top 10 acquisition function values and evaluate them in parallel) with a pool size $K = 50$.

TABLE A4: Comparison of various methods

methods (real-time threshold)	mobile GPU Speed (ms)	Car 3D detection		
		Easy	Moderate	Hard
pruning search only (100ms)	108	83.92	74.12	66.63
Ours (100ms)	97	85.20	75.57	68.37
Ours (90ms)	89	82.33	73.60	66.52

APPENDIX G ABLATION STUDY

We explore the effects of various pillar grid sizes and show the performance in Table A3. We can observe that larger grid size results in smaller pseudo-image input image sizes, thus the inference speed can be improved at the cost of detection performance degradation. For the grid size of 0.32m, the performance degradation is non-neglectable and thus we do not use the grid size of 0.32m.

We test the case with pruning search only instead of unifying network enhancement and pruning search as shown in Tab. A4. Under the same configuration, pruning search only can achieve a mAP of 74.89% with an average inference time of 108ms. Compared with the unified framework with 76.38% mAP and 97ms inference, we can see that incorporating network enhancement can further improve the detection and speed performance. We also note that although the real-time threshold is set to 100ms, without Winograd, pruning search still slightly violate the real-time requirement, demonstrating the acceleration performance of Winograd.

Moreover, as we increase the real-time requirement from 100ms to 90ms, the proposed method achieves a mAP of 74.15% with an average 89ms speed, demonstrating that the method prunes the model harder to improve speed, thus incurring detection performance degradation. We show the results in Table A4.